Ionic Self-Assembled Redox-Active Polyelectrolyte−Ferrocenyl Surfactant Complexes: Mesomorphous Structure and Electrochemical Behavior

Zhiyu Cheng, Biye Ren,* Ming Gao, Xinxing Liu, and Zhen Tong*

Research Institute of Materials Science, South China University of Technology, Guangzhou 510640, China

Received May 12, 2007; Revised Manuscript Received June 28, 2007

ABSTRACT: Redox-active polyelectrolyte−surfactant complexes (PSC) were prepared via the ionic self-assembly of sodium poly(styrenesulfonate) (PSS) and ferrocenyl surfactant, *n*-alkyl (ferrocenylmethyl)ammonium bromide (Fc*n*, $n = 8$, 12, 16, where *n* is the carbon number of the alkyl chain), in solution. The PSS−Fc*n* complex exhibited an ordered lamellar mesomorphous structure with the long period of $d = 2.49$, 2.94, and 3.74 nm for PSS−Fc8, PSS−Fc12, and PSS−Fc16, respectively. With increasing the length of surfactant alkyl chain, the stacking order was improved. Interestingly, in the solid complex, the ferrocenyl moieties formed H-aggregation showing an increase in the $\pi-\pi^*$ energy transfer of cyclopentadienes in the ferrocene moieties as known from the blue shift in the UV spectrum. These complexes showed higher thermal stability compared with their components due to the ionic interaction. Cyclic voltammogram (CV) measurements indicated that the electrode process of these redox-active complex films was diffusion-controlled and almost reversible or quasi-reversible at scan rates ranging from 0.02 to 4 V/s. Though the reversibility of the electrode process became worse for the PSS−Fc12 and PSS−Fc16 films than that for the PSS−Fc8, the redox peak current $|i_p|$ increased with increasing surfactant tail length in the complex because the more ordered packing in the complex film formed by longer surfactant tails was more favorable for the electrolyte diffusion and charge transfer as judged on values of the surface charge-transfer coefficient αn_α, standard rate constant K_s, and apparent diffusion coefficient D_{app} reflecting the electrode kinetics. The present results demonstrate that the electrochemical activity of the redox-active poly(styrenesulfonate)−ferrocenyl surfactant complex can be easily tuned by changing the surfactant tail length. Our work provides a simple and facile approach to the preparation of redox-active polymers with ordered mesomorphous structure by the ionic self-assembly.

Introduction

The technique of ionic self-assembly, i.e., the coupling of oppositely charged building blocks by electrostatic attraction, is a powerful tool to create new nanostructures and functional materials.[1] Considerable attention has been paid to the solid polyelectrolyte−surfactant complexes (PSC) of ionically self-assembled in the past decade due to their facile preparation and interesting properties.[2−12] Numerous studies have demonstrated that the supramolecular structure of the solid PSC can be tuned through charge density, flexibility, and hydrophobicity of the polymer chain as well as the nature of the surfactant, such as polar group, alkyl tail, and polar-to-nonpolar volume ratio.[6,8,13−15]

During recent years, many efforts have been devoted to the design of new functional PSC for special applications.[16−18] The main advantage of the solid PSC is that the ionic self-assembly provides a simple approach to tune properties of polymers without synthesizing new chemical species. For example, the ionic complexation of surfactants and the opposite charged conjugated polyelectrolytes, such as cationic poly(*p*-phenylene) (PPP)[3] and anionic poly(1,4-phenyleneethynylene carboxylate) (PPE)[17] and poly(2,5-methoxypropyloxysulfonate phenylenevinylene) (MPS−PPV),[16] tuned the optical and electronic properties of these component polymers. The ionic self-assembled complexes of polyelectrolytes with opposite charged fluorinated surfactants were particularly of interest for fabricating low-surface-energy materials due to the facility of preparation compared with other fluorine polymers. These low-surface-energy polyelectrolyte−fluorinated surfactant complexes promised to be used in protection of buildings and machines, high-performance coatings, and self-lubricating machine parts, etc.[2,19−23] It has been shown that not only the length of fluorinated tails in the surfactant but also the molar ratio of surfactant to polyelectrolyte with respect to the charged groups significantly influence the mesomorphous structure and surface tension of the polyelectrolyte−fluorinated surfactant complexes.[24]

On the other hand, organometallic materials became increasingly important in recent years in light of their uses as chemical sensors, electrocatalysts, modified electrodes, and photoelectronic devices.[25−31] The incorporation of organometallic moieties into the ultrathin film modified its optical, magnetic, and thermal properties. Ferrocene and its derivatives, as one of the most important organometallic electron mediators, play the role of electron transfer between redox matrix and electrode in electrochemical and biological sensors. The ferrocenyl surfactant was particularly of interest for supramolecular chemistry due to its synthetic convenience, hydrophobic character, and redox property.[32,33] The Langmuir−Blodgett (LB) films containing ferrocenyl surfactant showed potential applications in informational optics, communication, integrated optics, and electrochemical and biological sensors.[34−37] However, to our knowledge, no study on the interaction between polyelectrolyte and ferrocenyl surfactant as well as their ionic assembled complex has been reported up to now, except the interaction and aggregation behavior of ethyl(hydroxyethyl)cellulose and (11-ferrocenylundecyl)trimethylammonium bromide in solution.[38] Our main interest is focused on the mesomorphous structure of

* Corresponding authors: Tel (86)-20-87112886; Fax (86)-20-87110273; e-mail mcbyren@scut.edu.cn, mcztong@scut.edu.cn.

10.1021/ma071072e CCC: $37.00
Published on Web 09/14/2007

Scheme 1. Chemical Structures of Fc8, Fc12, and Fc16

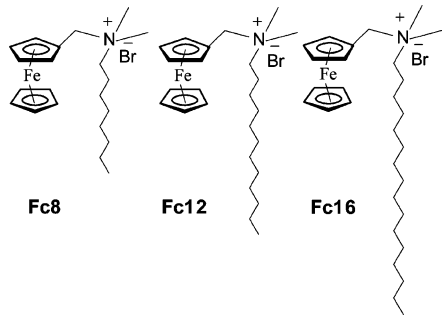

the PSC formed by the redox-active ferrocenyl surfactants and polyelectrolytes and the effect of mesomorphous structure on the electrochemical behavior as well as the electrode process of the redox-active polyelectrolyte−ferrocenyl surfactant complex. On the other hand, it is also expected that the redox-active polyelectrolyte−ferrocenyl surfactant complex would provide a new approach to immobilize the ferrocenyl moiety to polymer films through ionic-assembly to prevent ferrocene from losing slowly from its modified electrodes.

In the present study, ferrocenyl surfactants with different lengths of alkyl tails (Fc*n*, $n = 8$, 12, 16) (Scheme 1) were synthesized and then coupled to sodium poly(styrenesulfonate) (PSS) by ionic assembly in aqueous solution for the first time. The electrochemical behavior of the polyelectrolyte−ferrocenyl surfactant complexes was investigated with cyclic voltammetry (CV) measurements.

Experimental Section

Materials. Sodium poly(styrenesulfonate) (PSS, Aldrich, $M_w = 70\,000$) and (*N*,*N*-dimethylamino)methylferrocene (Alfa, purity >98 wt %) were used as received. 1-Bromooctane, 1-bromododecane, and 1-bromocetane (all from Shanghai Chemical Reagent Co.) were distilled under reduced pressure before use. Other reagents were all commercial chemicals of analysis grade and purified following the standard procedures. Water used for solutions was twice distilled.

Synthesis of Ferrocenyl Surfactants Fc8, Fc12, and Fc16. The ferrocenyl surfactants **Fc8**, **Fc12**, and **Fc16** were synthesized according to the literature procedure[39] with slight improvement. Synthesis of **Fc16** was taken as an example: To a three-neck 100 mL round-bottom flask with a Teflon-coated magnetic stirring bar, a mixture of (*N*,*N*-dimethylamino)methylferrocene (1.94 g, 8.0 mmol), NaI (4.40 mg), and 1-bromocetane (3.66 g, 12.0 mmol) in 50 mL of acetone was added. The mixture was refluxed under vigorous stirring for ~72 h in a N_2 atmosphere and then filtered at about 50 °C. The filtrate was cooled to room temperature, and then an orange-yellow precipitate was separated by filtration. The product was recrystallized twice from acetone/ether mixture of 1:1 in volume to produce 3.01 g of golden-yellow solid **Fc16** (yield: 68.4%). Anal. $C_{29}H_{50}NFeBr$: Calcd: C, 0.635; H, 0.092; N, 0.026. Found: C, 0.636; H, 0.093; N, 0.024. ^{1}H NMR, δ ($CDCl_3$, TMS, ppm): 0.88 (t, 3H, CH_3), 1.25−1.69 (m, 28H, (CH_2)$_{14}$), 3.2−3.4 (m, 8H, N(CH_3)$_2$CH_2), 4.37 (s, 9H, ferrocene cycle), 4.57 (s, 2H, FcCH_2). FT-IR (cm^{-1}): 3072, 2917, 2850, 1404, 1103, 1004, and 809. **Fc12** and **Fc8** were synthesized and identified similarly.

Complex Preparation. The complex PSS−Fc16 was prepared according to the following procedure: 0.80 g (1.46 mmol) of **Fc16** was dissolved in 10 mL of water at about 80 °C and slowly added dropwise into 10 mL of boiling water containing 0.30 g (1.46 mmol of repeat unit) of PSS under stirring. The yellow precipitate was separated by filtration, washed several times with hot water, and dried under vacuum at room temperature for 76 h. PSS−Fc8 and PSS−Fc12 were prepared following the same procedure. The chemical structure of PSS−Fc12 and its electron-transfer reaction equation are illustrated in Figure 1. For preparation of complex

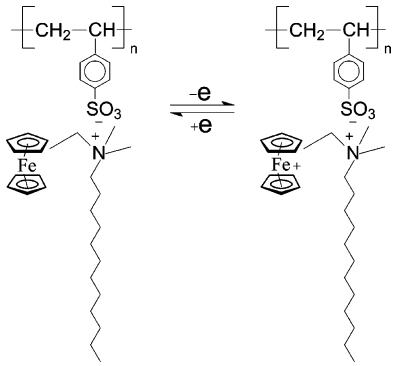

Figure 1. Chemical structure of PSS−Fc12 and its electron-transfer reaction.

films, the chloroform solution of the PSS−Fc*n* ($n = 8$, 12, 16) complex with 2×10^{-5} mol/L (counted for the ferrocenyl surfactant, the following is the same) was coated on a quartz glass at room temperature and dried for 48 h under vacuum at 60 °C.

Modification of Glassy Carbon (GC) Electrode with PSS−Fc*n* Complex. As a general procedure, first a Teflon-shrouded GC (geometric area 0.071 cm^2) electrode was burnished with 0.05 μm Al_2O_3 paste and then cleaned with pure water. Electrode was sonicated in ethanol and doubly distilled water after polish for 30 s, respectively. 4 μL solution of 0.068 mol/L PSS−Fc*n* ($n = 8$, 12, 16) complex in chloroform was spread evenly onto a freshly burnished GC electrode with a microsyringe. The coverage Γ of the complex on the electrode is estimated to be 3.88×10^{-6} mol/cm^2. A small bottle was sealed tightly covering the electrode to serve as a closed chamber to make chloroform evaporate slowly. The GC electrode modified with the PSS−Fc*n* complex film was then dried in N_2 atmosphere.

Measurements. Wide-angle X-ray diffraction (WAXD) and small-angle X-ray scattering (SAXS) measurements of the complex powder were performed in transmission geometry with an X'pert PRO diffractometer (40 kV and 40 mA) using Cu Kα radiation (wavelength $\lambda = 0.154$ nm) at room temperature. The 2θ ranged from 10° to 30° for WAXD, and the scattering vector s ranged from 0.113 to 1.5 nm^{-1} for SAXS, where $s = (2/\lambda) \sin \theta$. The scan step was 0.01° in 2θ with counting time of 1 s/step. The differential scanning calorimetry (DSC) was carried out with a 3−5 mg of sample in a 6 mm aluminum pan on a Netzsch DSC 204 under a nitrogen atmosphere at heating or cooling rate of 10 °C/min following the temperature sequence as room temperature → 140 °C → −60 °C → 140 °C. Thermogravimetry (TG) was measured with a Netzsch TG 209 under a nitrogen atmosphere at heating rate of 10 °C/min starting from room temperature up to 800 °C. Polarized optical microscope of Zeiss Axiophot was used with a Linkam hot stage. The carbon, hydrogen, and nitrogen contents (wt %) of the complex were determined with a Vario EL elemental analyzer. The ^{1}H NMR spectrum was obtained in $CDCl_3$ solution on a Varian INOVA 500NB spectrometer. UV−vis absorbance was measured with a Hitachi UV-3010 spectrophotometer. Cyclic voltammograms (CV) measurements were performed on a CHI 660 electrochemical workstation (CH Instruments, Shanghai) at room temperature under a nitrogen atmosphere in 0.1 M NaCl solution using a three-electrode system. The complex film modified GC was used as the working electrode, a platinum wire as the counter electrode, and saturated calomel as the reference electrode (SCE). The sweep rate was changed from 0.01 to 4 V/s, and the sweep range was from −0.4 to +1.0 V vs the SCE.

Results and Discussion

1. Structural Analysis. WAXD diagrams (data are not given here) show only one broad diffraction peak at $2\theta \approx 17.7°$ for all the PSS−Fc*n* ($n = 8$, 12, 16) complexes. Neither birefringence nor bright spot was observed from the three complex films with a polarization optical microscope at room temperature.

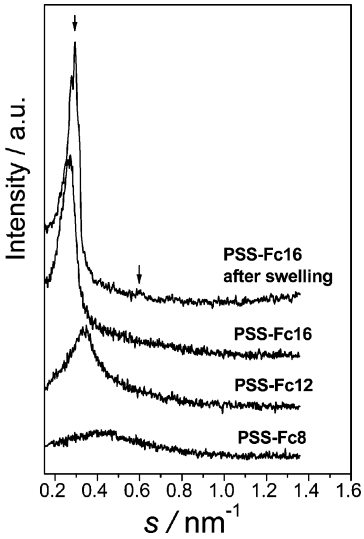

Figure 2. SAXS patterns of the complexes PSS−Fc8, PSS−Fc12, PSS−Fc16, and PSS−Fc16 after swelling with ethanol and dried, where $s = (2/\lambda) \sin \theta$.

These indicate the noncrystalline structure of these solid PSS−Fc*n* complexes. Figure 2 depicts the SAXS profiles of the complexes at room temperature. There is one reflection peak for each complex except that after swelling, indicating the existence of some long-distance-ordered structure in these complexes. The scattering vectors *s* of 0.40, 0.34, and 0.27 nm^{-1} for PSS−Fc8, PSS−Fc12, and PSS−Fc16 correspond to the long period of $d = 2.47$, 2.94, and 3.74 nm, respectively. Such diffraction data suggest a possible lamellar mesomorphous structure for the complexes, similar to that proposed by Antonitti et al. for the complexes of PSS and different alkyltrimethyammonium derivatives.[4] They suggested that the lamella was composed of two layers as polyions (polyelectrolyte and ionic head groups) and alkyl chains (tails) and the long period depends on the length and orientation of alkyl chains of surfactant. With the results of Antonitti et al.[4] and Ponomarenko et al.,[40] the thickness of the alkyl tail layer was estimated to be 1.09, 1.54, and 2.34 nm for PSS−Fc8,PSS−Fc12, and PSS−Fc16, respectively. These values are a bit larger than the tail length calculated for the stretched corresponding alkyl chains with the given carbon numbers because the increment of one carbon is about 0.125 nm to the long period for a completely stretched alkyl chain if the chain is perpendicular to the lamella.[4] Hence, the surfactant tails are interdigitately arranged in a monolayer in the complexes. Figure 2 also reflects that the scatting peak becomes narrower and higher as increasing chain length of the surfactant tails, indicating more perfect and ordered mesomorphous structure in the complex with a longer surfactant tail.

The lamellar mesomorphous structure was further verified by SAXS from the PSS−Fc16 complex film after swelling with ethanol and dried at 70 °C. Two peaks characterizing the lamellar mesomorphous structure were observed from the profile at the equidistant position as 1:2 in the d^{-1} scale (i.e., $d_{001} = 3.44$ nm and $d_{002} = 1.72$ nm) with a slight decrease in the long period from 3.74 to 3.44 nm. This result is due to the plasticizer effect of swelling solvent, which lubricates the segment motion to form a more order structure in the complex.

The chromophores can stack in parallel and form an angle α between the chromophore transition dipoles and the line passing through the dipole centers. For the H-aggregate α is greater than 54.7° and for the J-aggregate α is less than 54.7°.[41−43] It has been shown that the orientation of ferrocene (Fc) moiety within Fc16 monolayer formed H-aggregates due to the increase

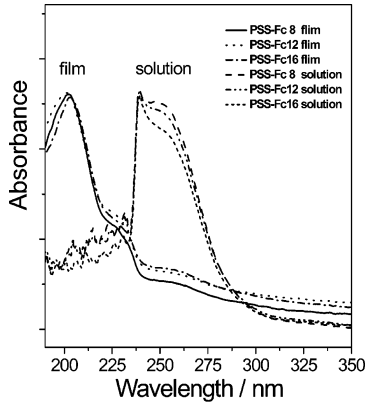

Figure 3. UV−vis spectra of the complexes PSS−Fc8, PSS−Fc12, and PSS−Fc16 in solution and solid film.

of the $\pi-\pi^*$ energy transfer of cyclopentadiene in ferrocene moieties.[44] An analogous observation was also reported by Shen et al.[45] on LB film containing Fc16 surfactant. It is therefore interesting whether the ferrocene (Fc) moieties form the H- or J-aggregate structure in these complexes. Figure 3 shows UV−vis spectra of the complexes PSS−Fc*n* ($n = 8$, 12, 16) in film and in chloroform solution. There are usually two peaks at ca. 240 and 440 nm in the UV−vis spectrum for the ferrocene and its derivatives, but the latter is very weak. As seen from Figure 3, the maximum absorbance of these complexes in chloroform solution appears at about $\lambda_{max} = 240$ nm, resulting from the $\pi-\pi^*$ electron transition of ferrocenyl moieties. In contrast, the solid films of the corresponding complexes present λ_{max} at about 203 nm, which blue-shifts about 37 nm from $\lambda_{max} = 240$ nm for the complexes in solution, suggesting the H-aggregate among ferrocene moieties causing an increase in the $\pi-\pi^*$ transfer energy of cyclopentadiene, similar to that reported by Shen et al.[45] on the Fc16 containing LB film. According to exciton-coupling theory developed by Kasha et al.,[41] noncovalent dimerization of molecules within an aggregate lowers the degeneracy of its excited electronic state compared to the uncoupled monomers. For H-aggregates, the higher electronic state carries all of the oscillating strength while transition to the lower electronic (exciton) state is forbidden. As the result, the absorption of the aggregate is blue-shifted in accordance with Kasha's rules.[46] The present behavior suggests that the ferrocenyl moieties of the complexes in solid film would form a close molecular packing as the H-aggregate; i.e., the cyclopentadienyl rings of Fc moieties are parallel to each other and tilted in the complex film organized by the ordered packing structure of alkyl tails. It is worth noting that this blue shift in the UV spectrum is identical for the three complexes PSS−Fc*n*, suggesting that the H-aggregate structure formed by the ferrocenyl moieties is independent of the tail chain length.

The possible structure of these complexes in solid state is schematically illustrated in Figure 4. For testing the conformation of the surfactant alkyl chains, we conducted solid ^{13}C-CP/MAS (cross-polarization/magic angle spinning)−TOSS (total suppression of sidebands) NMR on PSS−Fc12 at 25 °C. There were a strong peak at 23 ppm and a weak one at 25 ppm corresponding to the *gauche* and *trans* conformations for the alkyl chain, respectively, according to the results reported by Antonietti et al.[47] Therefore, only a small part of the alkyl chains exists in the trans conformation.

2. Thermal Properties. Thermal stability was investigated by TG analysis for the three complexes. The TG thermograms show that these complexes exhibit a two-step weight-loss process over 25−750 °C (Figure 5). The degradation temper-

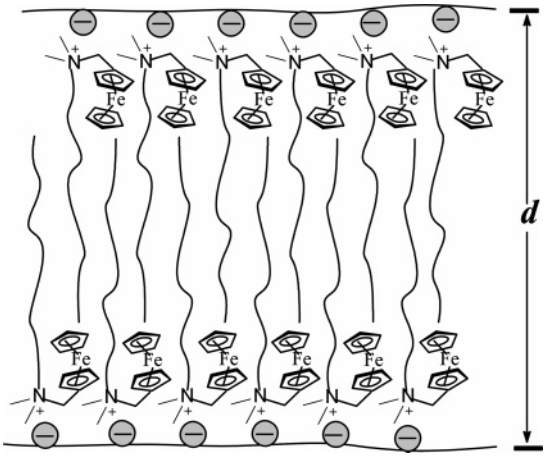

Figure 4. Possible structure model of the complex PSS−Fc*n*.

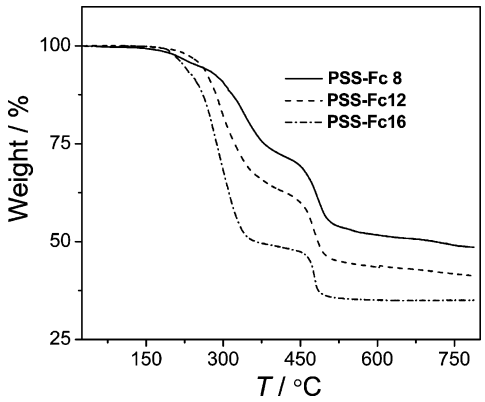

Figure 5. TG thermogram of the complexes PSS−Fc8, PSS−Fc12, and PSS−Fc16.

ature T_{d1} corresponding to the first maximum weight-loss rate for the three complexes PSS−Fc*n* (n = 8, 12, 16) is 308, 295, and 293 °C, respectively, while degradation temperature T_d for the surfactants Fc8, Fc12, and Fc16 is approximately 187, 190, and 206 °C, respectively (data not shown here). This indicates that the thermal stability of the complex is significantly enhanced when compared with the corresponding pure surfactant as the result of strong electrostatic interaction between $-SO_3^-$ (from PSS) and $\rangle N^+\langle$ (from ferrocenyl surfactant). The second maximum weight loss at about 480 °C is attributed to the degradation of PSS polymer in the complex. The corresponding degradation temperature T_{d2} significantly increases from 442 °C for the pure PSS (not shown here) to 480 °C for the complexes. In addition, no first-order transition appears in the DSC thermogram within −60 to 140 °C for these complexes, indicating noncrystalline structure for the complexes.

3. Electrochemical Behavior of the Complex. The present question is whether the ordered mesomorphous structure of the PSS−Fc*n* complexes would significantly affect the electrochemical activity of redox-active ferrocenyl moieties when incorporated into the interdigitating monolayer. In order to answer this question, we further studied electrochemical behavior of these complexes with the CV technique in 0.1 M NaCl solution at 25 °C. To obtain stable and reproducible CV data from the complex-coated GC electrode, the successive potential sweep from −0.4 to +1.0 V (vs SCE) at scan rate of 0.2 V/s was repeated many times until approaching a steady state; i.e., the voltammetric current was no longer decreased, and the peak separation was kept at a constant. Figure 6 depicts CV curves of the GC electrode modified with these complexes at a scan rate of 0.2 V/s within the potential range of −0.4 to +1.0 V in

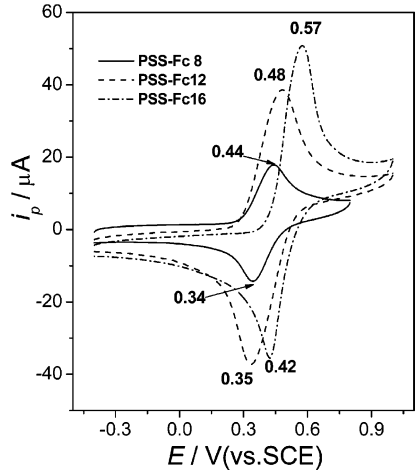

Figure 6. Cyclic voltammogram of the PSS−Fc8, PSS−Fc12, and PSS−Fc16 with scan rate of 0.2 V/s in 0.1 M NaCl solution at 25 °C.

0.1 M NaCl solution. A couple of redox peaks are observed from each curve. The anodic peak potential E_{pa} of the PSS−Fc*n* increases with chain length of the surfactant as 0.44, 0.48, and 0.57 V for n = 8, 12, and 16, respectively. The cathodic peak potential E_{pc} of the complexes is 0.34, 0.35, and 0.42 V for n = 8, 12, and 16, respectively. Thus, the potential difference ΔE ($= E_{pa} - E_{pc}$) is 0.10, 0.13, and 0.15 V for the complex PSS−Fc*n* with n = 8, 12, and 16. Generally, the kinetic reversibility of the redox couple can be assessed according to the separation of the anodic and cathodic peak potentials in CV.[48] The PSS−Fc*n* complex with longer surfactant tail demonstrates a less reversible redox process due to its higher ΔE. At the same time, the redox peak current $|i_p|$ of the complexes PSS−Fc12 and PSS−Fc16 is obviously higher than that of PSS−Fc8. The rapid increase of $|i_p|$ does not come from the increase in amount of the redox-active species because these complexes have almost the same coverage. In order to understand this interesting change, we observed the CV behavior of the PSS−Fc*n* complexes at different scan rates.

Figure 7 shows that the reduction peak E_{pc} of the complexes PSS−Fc*n* shifts to the left and the oxidation peaks E_{pa} shifts to the right with increasing the scan rate υ. So, the peak separation ΔE gradually increases with the scan rate. Taking the complex PSS−Fc8 as an example, E_{pc} shifts from 0.35 to 0.30 V and E_{pa} from 0.43 to 0.50 V when scan rate increases from 0.02 to 2 V/s. Thus, the ΔE increases from 0.08 to 0.2 V accordingly. Figure 8 depicts plots of ΔE against ln υ with the scan rate over 0.01−4 V/s for PSS−Fc12 and PSS−Fc16 (0.01−2 V/s for PSS−Fc8). When υ = 0.01−0.1 V/s, ΔE is almost independent of ln υ for the PSS−Fc8 but slightly increases for the other two complexes with increasing υ. While, when $\upsilon >$ 0.2 V/s, ΔE significantly grows with ln υ first exponentially and then linearly for all the three complexes. This suggests that electrode processes of the PSS−Fc*n*-modified GC electrode is almost reversible at lower scan rates but become quasi-reversible at higher scan rates, especially at $\upsilon >$ 0.2 V/s.[48,49]

Moreover, the redox peak current $|i_p|$ of the complex films gradually increases with increasing υ when $\upsilon <$ 0.2 V/s but significantly increases when $\upsilon >$ 0.2 V/s. It is well-known that the peak current $|i_p|$ linearly increases with the square root of the scan rate $\upsilon^{1/2}$ for a diffusion-controlled electrode process.[48,49] Figure 9 illustrates the observed anodic peak current i_{pa} for the three complexes PSS−Fc*n* with calculated fittings. The data for one modified electrode can be fitted with two straight lines of different slopes at υ = 0.01−0.1 and 0.2−4 V/s. The former corresponds to almost reversible process at lower scan rates and

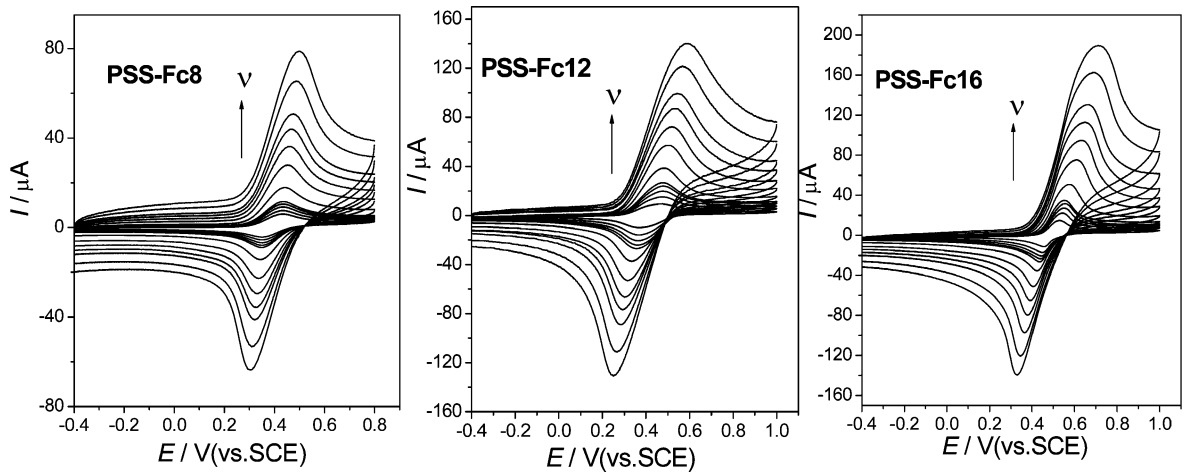

Figure 7. Cyclic voltammogram of the PSS−Fc8, PSS−Fc12, and PSS−Fc16 in 0.1 M NaCl solution at room temperature with different scan rates υ: 0.02, 0.04, 0.06, 0.08, 0.1, 0.2, 0.4, 0.6, 0.8, 1, 1.5, and 2 V/s.

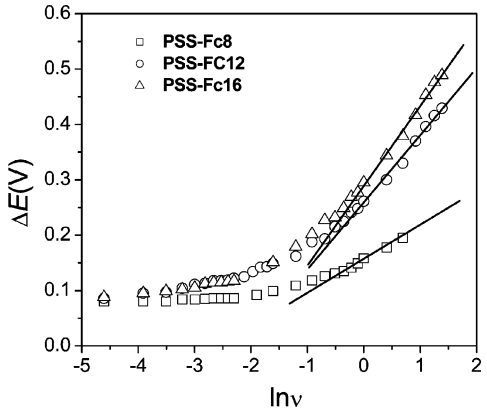

Figure 8. Plots of the peak separation ΔE of the complex PSS−Fc*n* (n = 8, 12, 16) against ln υ with the scan rate υ ranging 0.01 to 4 V/s in 0.1 M NaCl solution at 25 °C (scan rate range of 0.01−2 V/s for PSS−Fc8).

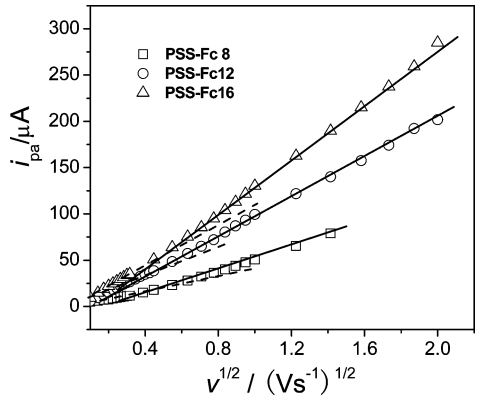

Figure 9. Dependence of the anodic peak current i_{pa} on the square root of potential scan rate $\upsilon^{1/2}$ for the complex PSS−Fc*n* (n = 8, 12, 16) at the scan rate ranging from 0.01 to 4 V/s in 0.1 M NaCl solution at 25 °C (scan rate range of 0.01 to 2 V/s for PSS−Fc8).

the latter to quasi-reversible process at higher scan rates (Figure 8). The fitting equations for i_{pa} and i_{pc} (cathodic peak current) are summarized in Table 1 for comparison. Hence, the CV results suggest that the electrode process of the PSS−Fc*n* films is diffusion-controlled.[48,49]

For a diffusion-controlled electrode process of the surface-immobilized redox species, i_p and ΔE can be expressed as follows:[49,50]

$$i_p = 0.4958nF(\alpha n_\alpha)^{1/2}\left(\frac{F}{RT}\right)^{1/2}AD_0{}^{1/2}C_0{}^*\upsilon^{1/2} \quad (1)$$

$$i_p = 0.227nFAC_0{}^*k^0 \exp\left[-\left(\frac{\alpha n_\alpha F}{RT}\right)(E_p - E^{0\prime})\right] \quad (2)$$

$$\Delta E = (RT/\alpha n_\alpha F)(\ln(RTK_s/2.184\alpha n_\alpha FD_0) - \ln \upsilon) \quad (3)$$

Here, i_p is the peak current in amperes, F is the Faraday constant, αn_α is the surface charge-transfer coefficient for the surface-immobilized redox species, R and T have their usual meaning, A is the film area covering the electrode surface in cm^2, D_0 is the apparent diffusion coefficient of the electroactive species in cm^2/s, C_0* is the concentration of the electroactive species in the film in mol/cm^3, υ is the potential scan rate in V/s, $E^{0\prime}$ is the apparent formal potential measured at low scan rate [$E^{0\prime} = (E_{pa} + E_{pc})/2$], and K_s is the standard rate constant in cm/s. We assumed that the film thickness d was ~10 μm, and then C_0* was obtained from $C_0{}^* = \Gamma/d$ because the concentration of the Fc*n* unit in the film was difficult to be measured directly. From eqs 1−3, we can calculate three important kinetic parameters, αn_α, K_s, and D_0, which indicate the electrochemical behavior, electrode process, and charge transfer. The αn_α and K_s and apparent diffusion coefficient D_{app} (for D_0 in the solution) so evaluated are listed in Table 1.

We can see from Table 1 that the αn_α values for the PSS−Fc12 and PSS−Fc16 films are 0.22 and 0.19, respectively, much smaller than 0.47 for the PSS−Fc8. The αn_α value is one of important factors to reflect the electron exchange efficiency on the electrode surface or the reversibility of the electrode process.[48] The smaller the αn_α value is, the less reversible the electrode process becomes. Therefore, the electrochemical reversibility of the complexes decreases in the order of PSS−Fc8, PSS−Fc12, and PSS−Fc16. In other words, the complex with longer surfactant tail has less reversible redox capability. On the other hand, the K_s and D_{app} values for PSS−Fc12 and PSS−Fc16 are much larger than those for PSS−Fc8. This means that the diffusion of counterions into the complex film and the charge transport from the film to the electrode are much faster for the PSS−Fc12 and PSS−Fc16 than that for the PSS−Fc8. The origin for these phenomena seems to be that the more ordered mesomorphous structure formed by the longer surfactant tails is more favorable to the counterion diffusion. The ultimate reason for this may lie in that the more ordered arrangement of alkyl tails in the complex would supply better channels for electrolyte diffusion and charge transfer. Hence, the larger K_s

Table 1. Fitting Equations for the Peak Separation ΔE, Peak Current i_p, against the Potential Scan Rate v and Kinetic Parameters αn_α, K_s, and D_{app} for the Complex-Modified GC Electrode

complex	range (V/s)	equation[a]	r[a]	$C_0^* \times 10^{-3}$ (mol/cm^3)	αn_α	$K_s \times 10^{10}$ (cm^2/s)	$D_{app} \times 10^{12}$ (cm/s)
PSS−Fc8	0.6−2	ΔE (V) = 0.156 + 0.055 ln v	0.9962				
	0.2−2	i_{pa} (μA) = −10.89 + 62.15$v^{1/2}$	0.9985	3.88	0.47	8.46	1.25
	0.2−2	i_{pc} (μA) = 8.96 − 50.54$v^{1/2}$	−0.9991			5.62	0.83
PSS−Fc12	0.6−4	ΔE (V) = 0.262 + 0.118 ln v	0.9962				
	0.2−4	i_{pa} (μA) = −9.03 + 106.20$v^{1/2}$	0.9997	3.88	0.22	13.16	7.72
	0.2−4	i_{pc} (μA) = 13.85 − 103.79$v^{1/2}$	−0.9982			12.56	7.37
PSS−Fc16	0.6−4	ΔE (V) = 0.296 + 0.137 ln v	0.9977				
	0.2−4	i_{pa} (μA) = −19.57 + 149.36$v^{1/2}$	0.9997	3.88	0.19	24.76	17.91
	0.2−4	i_{pc} (μA) = 14.78 − 106.97$v^{1/2}$	−0.9988			12.70	9.18

[a] Solid line in Figure 8 for ΔE and in Figure 9 for i_{pa}.

and D_{app} values result in a large increase in i_p for PSS−Fc12 and PSS−Fc16 complexes compared with PSS−Fc8.

Conclusions

New redox-active polyelectrolyte−surfactant complexes with different lengths of surfactant alkyl chains (PSS−Fc*n*, $n = 8$, 12, 16) were prepared through ionic self-assembly of PSS and ferrocenyl surfactants. These complexes exhibited an ordered lamellar mesomorphous and noncrystalline structure with increased packing order as the alkyl chain length of the surfactant increased. Ferrocenyl moieties in the complexes were found to form the H-aggregate due to the increase in $\pi-\pi^*$ energy transfer of cyclopentadienes as known from the blue shift in the UV spectrum. The electrode process of the PSS−Fc*n* complex films was diffusion-controlled, and the reversibility decreased with increasing scan rate v as judged by the relationship between the peak separation ΔE and ln v. On the other hand, the redox peak current $|i_p|$ increased with increasing the surfactant tail length in the complexes because the more ordered parking in the complex film formed by longer surfactant tails was more favorable for the electrolyte diffusion and charge transfer. Our results suggest that the electrochemical activity of the redox-active poly(styrenesulfonate)−ferrocenyl surfactant complex could be easily tuned through changing the length of the surfactant tails, which may provide a new kind of electrochemical sensor.

Acknowledgment. The financial support from the NSF of China (50673029 and 20534020), the Program for New Century Excellent Talents in University, and the NSF of Guangdong Province (05006561) is gratefully acknowledged.

References and Notes

(1) Faul, C. F. C.; Antonietti, M. *Adv. Mater.* **2003**, *15*, 673.
(2) Thünemann, A. F. *Prog. Polym. Sci.* **2002**, *27*, 1473.
(3) Thünemann, A. F.; Ruppelt, D.; Schnablegger, H.; Blaul, J. *Macromolecules* **2000**, *33*, 2124.
(4) Antonietti, M.; Conrad, J.; Thünemann, A. F. *Macromolecules* **1994**, *27*, 6007.
(5) Antonietti, M.; Conrad, J. *Angew. Chem., Int. Ed. Engl.* **1994**, *33*, 1869.
(6) Antonietti, M; Burger, C.; Effing, J. *Adv. Mater.* **1995**, *7*, 751.
(7) Zhou, S.; Chu, B. *Adv. Mater.* **2000**, *12*, 545.
(8) Macknight, W. J.; Ponomarenko, E. A.; Tirrell, D. A. *Acc. Chem. Res.* **1998**, *31*, 781.
(9) Ober, C. K.; Wegner, G. *Adv. Mater.* **1997**, *9*, 17.
(10) Ren, B.; Cheng, Z.; Tong, Z.; Liu, X.; Wang, C.; Zeng, F. *Macromolecules* **2005**, *38*, 5675.
(11) Ren, B.; Cheng, Z.; Tong, Z.; Liu, X.; Wang, C.; Zeng, F. *Macromolecules* **2006**, *39*, 6552.
(12) Ren, B.; Gao, F.; Tong, Z.; Liu, X.; Zeng, F. *Polymer* **2001**, *42*, 7291.
(13) Kogej, K.; Theunissen, E.; Reynaers, H. *Langmuir* **2002**, *18*, 8799.
(14) Pérez-Camero, G.; García-Alvarez, M.; Martínez de Ilarduya, A.; Fernández, C.; Campos, L.; Muñoz-Guerra, S. *Biomacromolecules* **2004**, *5*, 144.
(15) Kim, B.; Ishizawa, M.; Gong, J.; Osada, Y. *J. Polym. Sci., Part A: Polym. Chem.* **1999**, *37*, 635.
(16) Chen, L.; Xu, S.; McBranch, D.; Whitten, D. *J. Am. Chem. Soc.* **2000**, *122*, 9302.
(17) Thünemann, A. F.; Ruppelt, D. *Langmuir* **2000**, *16*, 3221.
(18) Ikkala, O.; Brinke, G. T. *Science* **2002**, *292*, 2407.
(19) Thünemann, A. F.; Schnöller, U.; Nuyken, O.; Voit, B. *Macromolecules* **1999**, *32*, 7414.
(20) Thünemann, A. F.; Schnöller, U.; Nuyken, O.; Voit, B. *Macromolecules* **2000**, *33*, 5665.
(21) Thünemann, A. F.; Lochhaas, K. H. *Langmuir* **1998**, *14*, 4898.
(22) Thünemann, A. F.; Lochhaas, K. H. *Langmuir* **1999**, *15*, 4867.
(23) Thünemann, A. F.; Kubowicz, S.; Pietsch, U. *Langmuir* **2000**, *16*, 8562.
(24) Ren, B.; Tong, Z.; Liu, X.; Wang, C.; Zeng, F. *Langmuir* **2004**, *20*, 10737.
(25) Yamamoto, T.; Saitoh, Y.; Anzai, K.; Fukumoto, H.; Yasuda, T.; Fujiwara, Y.; Choi, B. K.; Kubota, K.; Miyamae, T. *Macromolecules* **2003**, *36*, 6722.
(26) Oms, O.; Bideau, J.; Leroux, F.; Lee, A.; Leclercq, D.; Vioux, A. *J. Am. Chem. Soc.* **2004**, *126*, 12090.
(27) Wang, X.; Winnik, M. A.; Manners, I. *Macromolecules* **2002**, *35*, 9146.
(28) Rider, D. A.; Cavicchi, K. A.; Power-Billard, K. N.; Russell, T. P.; Manners, I. *Macromolecules* **2005**, *38*, 6931.
(29) Wang, X.; Winnik, M. A.; Manners, I. *Macromolecules* **2005**, *38*, 1928.
(30) Cyr, P. W.; Klem, E. J. D.; Sargent, E. H.; Manners, I. *Chem. Mater.* **2005**, *17*, 5770.
(31) Guldi, D. M.; Rahman, G. M. A.; Marczak, R.; Matsuo, Y.; Yamanaka, M.; Nakamura, E. *J. Am. Chem. Soc.* **2006**, *128*, 9420.
(32) Ifuku, S.; Tsujii, Y.; Kamitakahara, H.; Takano, T.; Nakatsubo, F. *J. Polym. Sci., Part A: Polym. Chem.* **2005**, *43*, 5023.
(33) Nath Bera, R.; Mallik, B. *Mol. Cryst. Liq. Cryst.* **2003**, *392*, 59.
(34) Mecheri, B.; Piras, L.; Ciotti, L.; Caminati, G. *IEEE Sens. J.* **2004**, *4*, 171.
(35) Aoki, A.; Miyashita, T. *J. Electroanal. Chem.* **1999**, *473*, 125.
(36) Aoki, A.; Abe, Y.; Miyashita, T. *Langmuir* **1999**, *15*, 1463.
(37) Chai, X. D.; Yang, W. S.; Lu, R.; Cao, Y. W.; Lu, N.; Jiang, Y. S.; Bai, Y. B.; Li, T. J. *Supramol. Sci.* **1998**, *5*, 679.
(38) Hays, M. E.; Abbott, N. L. *Langmuir* **2005**, *21*, 12007.
(39) Saji, T.; Hoshino, K; Aoyagui, S. *J. Am. Chem. Soc.* **1985**, *107*, 6865.
(40) Ponomarenko, E. A.; Waddon, A. J.; Bakeev, K. N.; Tirrell, D. A.; Macknight, W. J. *Macromolecules* **1996**, *29*, 4340.
(41) Kasha, M. *Molecular Excitons in Small Aggregates*; Plenium Press: New York, 1976.
(42) McRae, E. G.; Kasha, M. The Molecular Exciton Model. *Physical Processes in Radiation Biology;* Academic Press: New York, 1964; p 23.
(43) Bohn, P. W. *Annu. Rev. Phys. Chem.* **1993**, *44*, 37.
(44) Fukuda, K.; Nakahara, H. *Colloids Surf., A* **1995**, *102*, 57.
(45) Shen, Y.; Xia, B.; Xie, A.; Tang, Y. C *Colloids Surf., A* **2005**, *252*, 21.
(46) Chowdhury, A.; Yu, L.; Raheem, I.; Peteanu, L.; Liu, L. A.; Yaron, D. J. *J. Phys. Chem. A* **2003**, *107*, 3351.
(47) Antonietti, M.; Radloff, D.; Wiesner, U.; Spiess, H. W. *Macromol. Chem. Phys.* **2006**, *197*, 2713.
(48) Bard, A. J.; Faulkner, L. R. *Electrochemical Methods*; John Wiley & Sons: New York, 1980; Chaper 6.
(49) Wang, X.; Wang, L.; Wang, J.; Chen, T. *J. Phys. Chem. B* **2004**, *108*, 5627.
(50) Laviron, E. *J. Electroanal. Chem.* **1979**, *101*, 19. Laviron, E.; Roulier, R. *J. Electroanal. Chem.* **1980**, *115*, 65.

MA071072E